# Structural and Optical Properties Of Nanoparticle ZnO Deposited By Spray Pyrolysis

Y. Bakha*, H. Khales, R. Serhane, A. Smatti

*Centre for Development of Advanced Technologies, Cité 20 Août 1956, Baba Hassen, BP. 17, Algiers DZ-16303, Algeria.*

*\* Corresponding author. Dr Y. Bakha email: ybakha@cdta.dz.*

**Abstract.** We present in this paper the deposition of nanoparticle zinc oxide (ZnO) by a simplified chemical spray process. A deposition was carried on glass substrates at different temperatures, to determine the ZnO optimal parameters. The characterization results by X-ray diffraction (XRD), scanning electron microscopy (SEM) and transmittance, shows that the obtained thin films are in good agreement with the reported ZnO properties. The films exhibit a hexagonal wurtzite structures. Scanning electron microscopy (SEM) measurements showed that the surface morphology of the films changed with temperature deposition. The studies demonstrated that the ZnO film had a transmission of about 85% and energy gap of 3.2eV to 3.3eV with increasing temperatures from 300°C to 350°C. The optical band gap of deposited films at temperatures of 400°C to 500°C increased from 3.56eV to 3.76eV.

*Keywords.* Zinc oxide; Nanoparticle; Optical properties; Chemical deposition; Spray pyrolysis.

## INTRODUCTION

Zinc oxide (ZnO) is most attractive materials used in several works since many years for his various and interesting properties. ZnO is one of the most important binary II-VI semiconductors compounds used as thin films in different areas. For his high optical transmittance in the visible light region, the ZnO is used as transparent conductive film and window materials in solar cell applications (Ozgur et al., 2010; Yang et al., 2008). He attracted much more interest in the electronics devices such optoelectronic devices in light-emitting diodes (LEDs) (Ozgur et al., 2010; Sepulveda-Guzman et al., 2010) and laser diodes (Chu et al., 2008). Due to his higher piezoelectric coupling coefficient property he is used in acoustic wave devices as piezoelectric transducers, such bulk and surface acoustic wave devices (BAW and SAW) and resonators for radio-frequency communications (Fu et al., 2015). For MEMS applications, the ZnO is proposed in many devices like in piezoelectric MEMS vibration energy harvesters (Wang and Du, 2015), microphones (Lee et al., 2008; Li et al., 2017), microfluidic systems and biomedical applications (Fu et al., 2007a, 2017b).

Recently, much interest is observed for ZnO as a nanostructure material and as nanostructure electrode material (Lao et al., 2002; Sood et al., 2011; Wang, 2004; Xia et al., 2016). Other uses of ZnO are as sensitive layer for various gas sensing applications; the doped or undoped thin film or nanostructured film are coated on various supports like on the top of MEMS micro cantilever surface (Aprilia et al., 2015; Kilinc et al., 2014), SAW sensors (Guo et al., 2017), metal oxide semiconductors (MOX) gas sensors and in a portable electronic nose (E-nose) (Wetchakun et al., 2011). The sensitivity can concern various target gases such as example; methane, Liquefied petroleum gas LPG, CO2, CO, NO2, H2S, ethanol and methanol.

Naturally, the ZnO has hexagonal wurtzite structure along the plane (002). For enhancing films sensitivity, the films must have high electrical resistivity associated with a small crystallite size and thickness (Nunes et al., 2002). These physical parameters are dependent on the conditions and parameters of deposition. Therefore, it is necessary to control fabrication process to obtain the optimal ZnO properties. Several techniques have been used for the production of ZnO thin films such as reactive magnetron sputtering (Li and Gao, 2004; Lee et al., 2008; Yang et al., 2012), pulsed laser deposition (Zhao and al., 2005), molecular beam epitaxy (Chen et al., 1998; Look et al., 2002), vapor deposition (Minegishi et al., 1997), sol–gel (Znaidi et al., 2012a, 2013b), spray-pyrolysis (Ashour et al., 2006; Bakha et al., 201; Larbah et al., 2015; Ilican et al., 2007) and chemical spray (Vayssieres, 2003; Zhao et al., 2006). The chemical spray process used in previous work (Bakha et al., 2011), still advantageous for his simplicity, low cost and process yield.

Our purpose is to study properties of zinc oxide thin films prepared by chemical deposition with different temperatures in order to see the influence of heating during process on the structural, morphological and optical properties. These properties are considered through the characterization by X-ray diffraction (XRD), scanning electron microscopy (SEM) and transmittance.

## EXPERIMENTAL DETAILS

ZnO thin films have been deposited by spray pyrolysis technique with (0.08M), using a starting solution of Zinc acetate dehydrate (Zn (CH3CO2)2, 2H2O) diluted in methanol 99.99% as solvent (CH3OH) on glass substrates Pyrex ®_ pieces (75×25×1mm3). This substrates were emerged in ultrasonic bath (in different solution such as ethanol, acetone) for (10-20) minutes and finally washed by distilled water, in order to clean them.

The spray pyrolysis system is composed of spray gun nozzle, air compressor, thermocouple, substrate heater; the spray nozzle is fixed at an appropriate distance from the substrate (27cm). This distance was chosen based on optimization of parameters. The solution is spraying as very small droplets in order to have homogenous thin films. During the spraying process, the substrates were heated on an electrically heated plate.

## RESULTS AND DISCUSSION

In this paper, we discussed the influence of temperature on the structural, optical and electrical properties of ZnO deposited films at several temperatures in the range of 300°C to 500°C. The surface morphologies of films were examined by electronic microscopy (SEM) (JEOL). The investigation of structural properties of the ZnO thin films was performed through X-ray diffraction (XRD) D8 Advance Bruker, using the Cu K☐ radiation (☐=1.54056A).

### Scanning electron microscopy (SEM)

Figure 1 Shows the scanning electron microscope (SEM) images of ZnO thin films deposited at (a) T=300°C, (b) T=350°C, (c) T=400°C and (d) T=500°C. The surface of the thin films

displays a homogenous appearance in all scanned areas. The films also showed the increasing of the crystallite size, they are given respectively from (a) T=300°C, (b) T=350°C and (c) T=400°C, more than the crystallites size are decreasing.
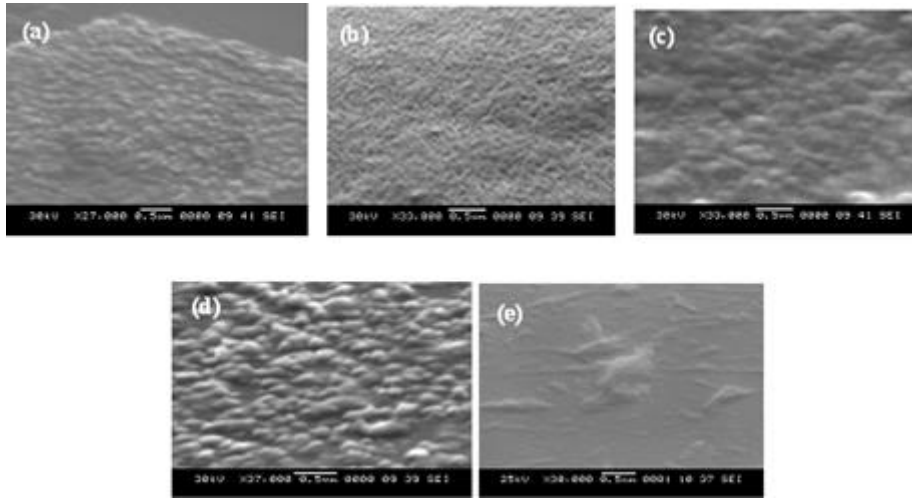


Fig. 1. SEM images of ZnO thin film deposited at (a) T=300°C, (b) T=325°C, (c) T=350°C, (d) T=400°C and (e) T=500°C.
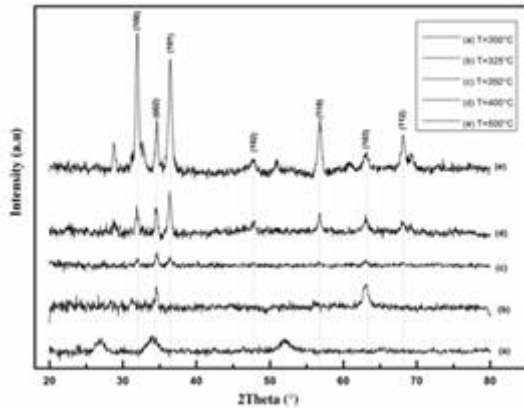
## X-ray diffraction characterization



Fig. 2. XRD patterns of ZnO thin films deposited at (a) T=300°C, (b) T= 325°C (c) T=350°C (d) T=400°C and (e) T=500°C.

The crystallite size of the thin films was determined from the XRD patterns of ZnO thin films illustrated in Figure 2, using the Scherer's formula (Scherrer, 1918):

$$D = \frac{K\lambda}{\beta \cos \theta_{(hkl)}} \qquad (1)$$

Where D is the crystallite size, $\lambda$=0.15406 nm the mean wavelength of Cu K$\alpha$ radiation, $\beta$ the full-width at half maximum (FWHM) of Bragg peak observed at Bragg angle $\theta$(rad), K=0.9. The calculated values of D are shown in Table 1. The average grain sizes in different orientations were determined from the diffraction peak width. For the (002) peak, the grain sizes are increasing when the substrate temperature increases.

The layer dislocation density $\delta$ is a parameter that presents directly the imperfection of the crystal lattice, and which corresponds to the dislocation line length by volume unit of the crystal. Unlike gaps ($O^{2-}$) or interstitial atoms ($Zn^{2+}$), dislocations are imperfections out of equilibrium. The density of dislocation is written (Yang et al., 2008):

$$\delta = \frac{1}{D^2} \qquad (2)$$

The results are shown in Table 1. The lattice constants (a) and (c) for the ZnO deposited films were calculated using equation (Lupan et al., 2010):

$$\frac{1}{d_{hkl}} = \frac{a}{\sqrt{\frac{4}{3}(h^2+k^2+hk)+l^2\frac{a^2}{c^2}}} \qquad (3)$$

The calculated lattice parameters are reported in Table 1. The lattice parameters of ZnO thin films prepared at different temperatures are characteristic of a hexagonal unit wish agree well with literature a=3.251Å and c=5.223Å. The ratio a/c for the ZnO thin films are given in table 1. It can be seen that the best a/c ratio which agree well with literature are for films deposited at T= 350°C, 400°C, 500°C.

The stress state in the layer can be determined by XRD analysis. According to biaxial stress model, the stress σ along the c-axis perpendicular to the plane of the substrate is calculated from the lattice strain (ε parameter) in the same direction. This lattice strain ε (%) was estimated from X-ray line broadening using equation (Muchuweni et al., 2017):

$$\varepsilon(\%) = \frac{c_{TF} - c_0}{c_0} \, 100 \qquad (4)$$

With $c_{TF}$ is the lattice parameters of the deposited thin films and $c_0$ is the lattice constant of the unconstrained layer ($c_0$=5.2Å) (Muchuweni et al., 2017). The residual stress σ parallel to the layer surface is expressed as (Muchuweni et al., 2017):

$$\sigma(GPa) = -233 \ \varepsilon \qquad (5)$$

This shows the interest of the measurement of the C lattice parameter, since it allows knowing the stresses state in the deposited layer towards the different directions.

We summarize in the Figure 3 the structural properties obtained on the deposited layers (in room conditions) and at substrate temperatures range of 300°C to 500°C. It can be seen, from this figure, that the deposition temperature influences the different structural parameters. We notice a decrease of the c lattice parameter as a function of the temperature. The position 2☐ of the (002) peak also follows the same variation as a function temperature. All the elaborated layers exhibit a value of 2θ  (corresponding to the 002 ZnO peaks) greater than that obtained on powdered ZnO (wish is 2θ=34.42°) for the deposited films at T=300°C to T350°C, we can see clear that more 400°C the peak position change to (100). This can be explained by the fact that all deposited layers have an undergone compression stresses in the crystal growth direction. This phenomenon is confirmed through the residual stress σ of films which systematically have a positive sign, indicating that the materials are under tensile stresses perpendicularly to the c-axis.

It should be noted that all ZnO layers have been deposited on the same type of amorphous glass substrate. The influence of the coherence constraint between the thin films and substrate has not been taken into account. When a layer is deposited at a given temperature, growth constraints and thermal stresses appear.

We can see that we have the nanoparticle material deposited by simple technique.

Table 1. The structural parameters of the deposited ZnO thin films.

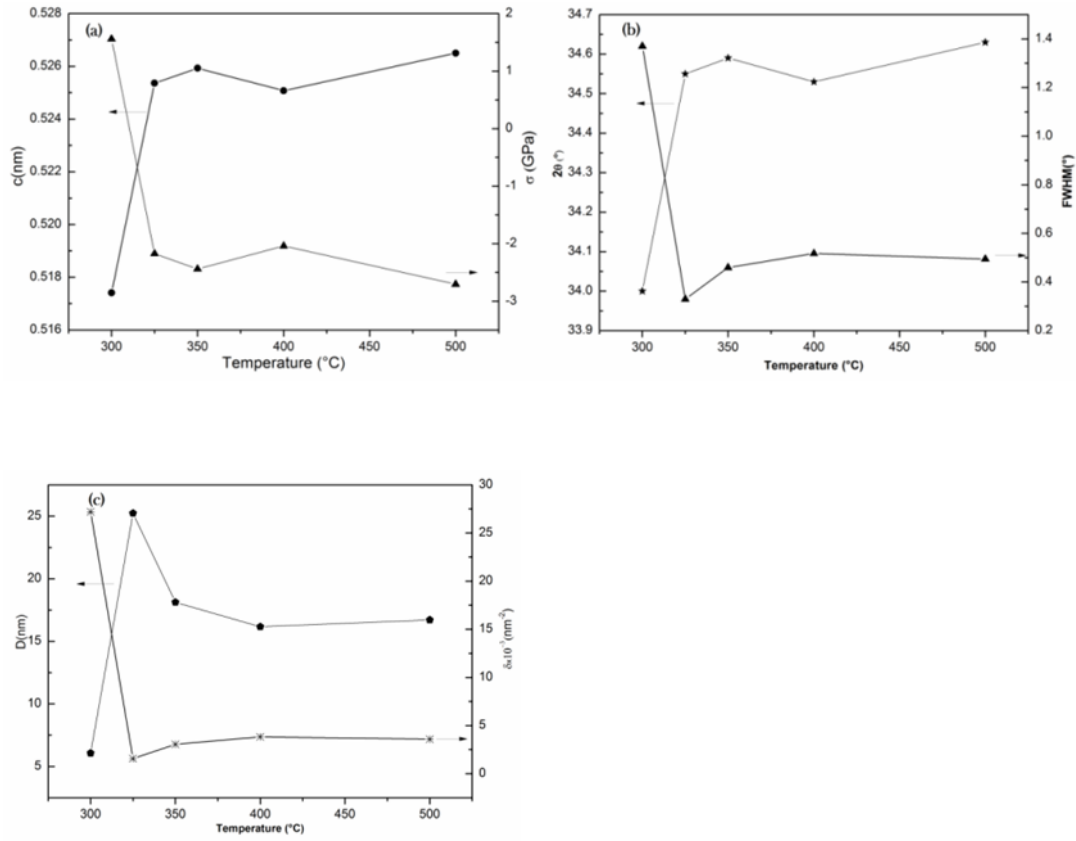| T(°C) | $2\theta_{hkl}$ | FHWM | D (nm) | $d_{hkl}$ (Å) | a(Å) | c(Å) | a/c | σ (GPa) | $\delta(nm^{-2})$ |
|---|---|---|---|---|---|---|---|---|---|
| 300 | 34.02 | 1.37 | 6.06 | 2.635 | 3.257 | 5.270 | 0.616 | -2.850 | 0.02720 |
| 325 | 34.55 | 0.329 | 25.25 | 2.594 | 3.267 | 5.188 | 0.629 | 0.790 | 0.00157 |
| 350 | 34.59 | 0.459 | 18.11 | 2.591 | 3.267 | 5.183 | 0.623 | 1.050 | 0.00305 |
| 400 | 36.37 | 0.517 | 16.16 | 2.468 | 3.232 | 5.198 | 0.622 | 0.659 | 0.00383 |
| 500 | 31.95 | 0.494 | 16.71 | 2.799 | 3.232 | 5.177 | 0.624 | 1.310 | 0.00358 |

Fig. 3. ZnO on glass structural parameters, obtained by DRX analysis versus the substrate temperature -a) Lattice parameters constant c and the corresponding residual stress σ, -b) (002) Bragg angle (2θ) and the corresponding FWHM and -c) Crystallite size D and the corresponding dislocation density δ of the layer.

**OPTICAL TRANSMISSIONS**

The transmittance spectra of the deposited films ZnO at different temperature from T=300°C to T=350°C and from 400°C to 500°C on glass substrate are shown in Figure 4. It is found that the transmissivity is above 85%. Based on the transmittance spectra, the optical band gap with direct transition Eg was obtained by extrapolating the linear portion of the plot $(\alpha h\nu)^2$ versus $(h\nu)$ to α=0 according to the following equation (Muchuweni et al., 2017):

$$\alpha = A(h\nu - Eg)^{1/2} \qquad (6)$$

Where hν is the photon energy, Eg is the band gap, A is the edge parameter for direct gap material.
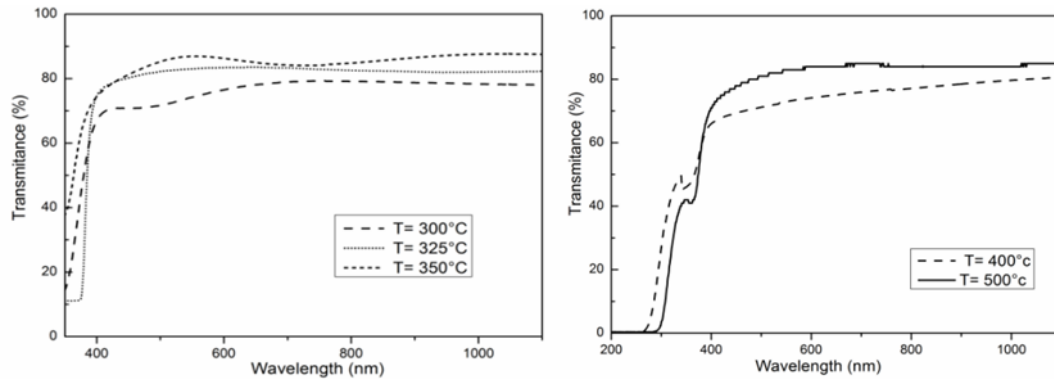
Fig. 4. Transmittance spectra of ZnO thin films deposited at:   T=300°C, T=325°C and T=350°C.T=400°C, T=500°C.
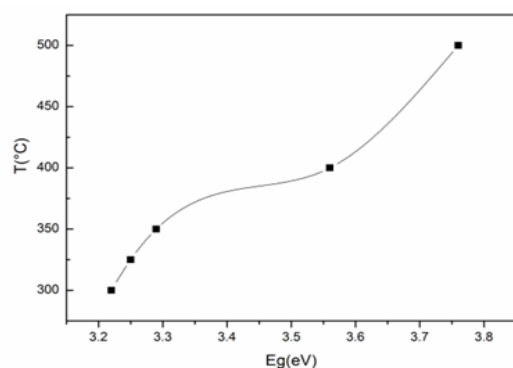


Fig. 5.  Evolution of the of band gap as a function of temperature of deposition
The evolution of the of band gap as a function of temperature of deposition is illustrated in Figure 5 while the band gap increases from 3,2eV to 3,76eV at high temperature.

## CONCLUSIONS

Nanoparticle of Zinc oxide (ZnO) has been deposited by simple method spray pyrolysis in ambient atmosphere on glass substrate. SEM image revolves that the surface of the thin films displays a homogenous appearance in all scanned areas. X-ray diffraction analysis of samples shows that its structure is hexagonal with an increasing of the crystallite size of the particles deposited at low temperature and decrease for the samples deposited at high temperature. Currently, research work is being carried out to better understand the mechanism of formation of these films, and the dependency of properties like size, shape and chemical constitution on the synthesis parameters. The lattice parameters are larger than that of standard ZnO, which shows that these films are constrained. Optical transmittance of ZnO thin films were investigated by using UV-VIS spectroscopy, the transmittance is above 85%.

## ACKNOWLEDGMENTS

## REFERENCES

Aprilia L., Nuryadi, R., Mayasari R. D., Gustiono D., Raharjo, J., Deni Y., Yuliarto D., Iqbal B. M., Hartanto D., 2015. IEEE International Conference on Quality in Research. 151-154.

Bakha Y., Djeridane Y., Aouimeur W., Menasri L., Smatti A., Hamzaoui S., 2014. IEEE 9th International Conference on Design and Test Symposium. 1-3.

Chala S., Sengouga N., Yakuphanoğlu F., Rahmane S., Bdirina M., Karteri İ., 2018. Energy. 164, 871–880.

Chen Y., Bagnall, D. M., Koh, H. J., Park, K. T., Hiraga, K., Zhu, Z., Yao, T., 1998. Journal of Applied Physics. 84(7), 3912-3918.

Chu S., Olmedo M., Yang Z., Kong J., Liu J., 2008. Applied Physics Letters 93(18), 181106. Fu Y. Q., Luo J. K., Nguyen N. T., Walton A. J., Flewitt A. J., Zu X. T., Li, Y., McHale G.,

MatthewsA., Iborra E., Du H., 2017. Progress in Materials Science. 89, 31-91.

Iftimie N., Steigmann R., Savin A., Tugui C.A., Munteanu C., 2018. IOP Conference Series: Materials Science and Engineering. 374, 012070.

Joshi L.P., Poudel Y., Nakarmi M.L., Niraula P.R., Shrestha S.P., 2017. Journal of Nepal Physical Society. 4, 1.

Karzazi O., Soussi L., Louardi A., El Bachiri A., Khaidar M., Monkade M., Erguig H., Taleb M., 2019. Superlattices and Microstructures. 127, 61–65.

Kilinc N., Cakmak O., Kosemen A., Ermek E., Ozturk S., Yerli Y., Ozturk Z.Z., Urey H., 2014. Sensors and Actuators B: Chemical. 202, 357-364.

Larbah Y., Adnane M., Sahraoui T., 2015. Materials Science-Poland. 33(3), 491-496.

Li J., Wang C., Ren W., Ma J., 2017. Smart Materials and Structures. 26(5), 055033.

Li W., Guo Y., Tang Y., Zu X., Ma J., Wang L., Fu Y. Q., 2017. Sensors. 17(5), 1142.

Look D. C., Reynolds D. C., Litton C. W., Jones R. L., Eason D. B., Cantwell G., 2002. Applied physics letters. 81(10), 1830-1832.

Luo C.-Q., Ling F.C.-C., Rahman M.A., Phillips M., Ton-That C., Liao C., Shih K., Lin J., Tam H.W., Djurišić A.B., et al., 2019. Applied Surface Science. 483, 1129–1135.

Lupan O., Pauporté T., Chow L., Viana B., Pellé F., Ono L. K., Ono L.K., Roldan Cuenya B., Heinrich H. 2010. Applied Surface Science. 256(6), 1895-1907.

Mahmoud F.A., Ahmed N. 2018. Journal of Semiconductors. 39, 093002.

Minegishi K., Koiwai Y., Kikuchi Y., Yano K., Kasuga M., Shimizu A., 1997. Japanese Journal of Applied Physics. 36(11A), L1453.

Muchuweni E., Sathiaraj T. S., Nyakotyo H., 2017. Heliyon 3(4), e00285.

Nunes P., Fortunato E., Tonello P., Fernandes F. B., Vilarinho P., Martins R., 2002. Vacuum. 64(3-4), 281-285.

Ozgur U., Hofstetter D., Morkoc H., 2010. Proceedings of the IEEE. 98(7), 1255-1268.

Scherrer P., 1918. Nachr. Ges. Wiss. Göttingen 2, 98-100.

Sepulveda-Guzman S., Reeja-Jayan B., De la Rosa E., Ortiz-Mendez U., Reyes-Betanzo C., Cruz-Silva R., Jose-Yacaman M., 2010. Applied Surface Science. 256(11), 3386-3389.

Suma N.M., N Prasad M.V., Gaddam V., Rajanna K., Nayak M., 2019. Journal of Pure Applied and Industrial Physics. 9, 1–7.

Tao K., Yi H., Tang L., Wu J., Wang P., Wang N., Hu L., Fu Y., Miao J., Chang H., 2019. Surface and Coatings Technology. 359, 289–295.

Theerthagiri J., Salla S., Senthil R.A., Nithyadharseni P., Madankumar A., Arunachalam P., Maiyalagan T., Kim H.-S., 2019. Nanotechnology. 30, 392001.

Wang P., Du H., 2015. Review of Scientific Instruments. 86(7), 075002.

Wetchakun K., Samerjai T., Tamaekong N., Liewhiran C., Siriwong C., Kruefu V., Wisitsoraat A., Tuantranont A., Phanichphant S., 2011. Sensors and Actuators B: Chemical. 160(1), 580-591.

Xia Y., Wang J., Chen R., Zhou D., Xiang L., 2016. Crystals. 6(11), 148.

Yang L., Duponchel B., Cousin R., Gennequin C., Leroy G., Gest J., Carru J. C., 2012. Thin Solid Films. 520(14), 4712-4716.

Zhang D., Dong G., Cao Y., Zhang Y., 2018. Journal of Colloid and Interface Science. 528, 184–191.

Zhao X., Li S., Ai C., Liu H., Wen D., 2019. Micromachines. 10, 212.